Computer Animation and Virtual Worlds

WILEY

SPECIAL ISSUE PAPER

CASAXR 26: International Conference on Computer Animation, Social Agents, and Extended Reality

From SVG to DSVG: Leveraging Foveal Visual Cues to Mitigate Cybersickness in Redirected Walking

Xinda Liu[1] | Yongbo Tang[1] | Xiaoning Liu[1] | Pengbo Zhou[2] | Guohua Geng[1]

[1]College of Computer Science, Northwest University, Xi'an, China | [2]School of Arts and Communication, Beijing Normal University, Beijing, China

Correspondence: Xiaoning Liu (xnliu@nwu.edu.cn)

Received: 15 April 2026 | **Revised:** 13 May 2026 | **Accepted:** 15 May 2026

Keywords: cybersickness | redirected walking | virtual reality

ABSTRACT

Redirected Walking (RDW) effectively extends the navigable area of virtual environments but frequently induces cybersickness due to vestibular-visual conflicts. To mitigate this, this study proposes a hierarchical visual guidance framework. We first introduce a Steering Visual Guidance (SVG) model, which employs a grid-based pattern to provide a stable visual reference frame. While effective, our evaluation revealed that the static, full-field nature of SVG can occlude the user's view and reduce visual clarity. To address this limitation, we optimized the model into Dynamic Steering Visual Guidance (DSVG). Grounded in the physiological principles of central and peripheral vision, DSVG dynamically renders stability cues exclusively within the foveal region, fading them in the periphery based on retinal sensitivity. A user study demonstrates that both SVG and DSVG significantly reduce subjective discomfort and physiological markers of sickness compared to a control condition without cues. Crucially, DSVG achieves sickness mitigation comparable to SVG while reducing visual occlusion by approximately 70%. These findings suggest that DSVG offers a robust, occlusion-minimizing solution for deploying RDW in constrained physical spaces.

1 | Introduction

Redirected Walking (RDW) serves as a pivotal technique in Virtual Reality (VR), enabling users to explore expansive virtual environments within constrained physical spaces by imperceptibly manipulating walking trajectories through translational and rotational gains [1, 2]. By subtly decoupling the virtual camera from physical motion, RDW creates the illusion of an infinite virtual space. However, the widespread adoption of RDW is fundamentally constrained by cybersickness, a physiological response triggered by the discrepancy between vestibular signals and visual feedback [3]. This sensory conflict disrupts neural integration, manifesting as dizziness, nausea, and disorientation, thereby severely limiting the duration and quality of VR immersion.

While mitigation strategies such as dynamic Field-of-View (FOV) restriction and saccadic suppression have been proposed [4, 5], they often compromise the sense of presence or prove ineffective in dynamic locomotion scenarios. Moreover, the severity of cybersickness is positively correlated with gain amplitudes; higher gains—essential for efficient redirection in smaller rooms—invariably induce more intense discomfort. Consequently, a critical challenge remains: How can we mitigate cybersickness in RDW without sacrificing the user's field of view or redirection efficiency?

To address this challenge, this study proposes a hierarchical visual guidance framework grounded in the physiological principles of human vision—specifically the distinct roles of central and peripheral vision. Building upon the classic concept of an

Abbreviations: DSVG, dynamic steering visual guidance; RDW, redirected walking; SD, standard deviation; SSQ, simulator sickness questionnaire; SVG, steering visual guidance.

independent visual background (IVB) introduced by [6], we first establish a Steering Visual Guidance (SVG) baseline. While traditional IVBs utilize a static grid to provide a stable reference frame, SVG extends this principle by dynamically coupling the grid's velocity to the user's real-time rotation gains, thereby accommodating the active locomotion of RDW.

However, our formative evaluation revealed a critical trade-off: while SVG effectively alleviates sickness, its static, full-field nature tends to occlude the virtual environment and degrade immersion. To resolve this conflict between visual comfort and FOV occlusion, we optimized the baseline into Dynamic Steering Visual Guidance (DSVG). This represents the core contribution of our work. Leveraging eye-tracking technology, DSVG adopts a gaze-contingent approach. It dynamically renders stability cues exclusively within the foveal region while fading them in the periphery based on retinal sensitivity. This bio-inspired optimization ensures that the visual cues remain perceptually salient for stability but minimizes visual interference with the virtual environment.

Our user study demonstrates that this hierarchical approach offers a robust solution. DSVG achieves sickness mitigation comparable to, or better than, SVG, while significantly reducing visual occlusion. This work provides empirical evidence that aligning visual feedback with the natural processing characteristics of the human eye can extend the comfortable duration of RDW.

By extending established visual mitigation principles with modern eye-tracking capabilities, the specific practical contributions of this paper are summarized as follows:

1. We propose a practical optimization framework that progresses from a foundational SVG baseline to a gaze-contingent DSVG model. By systematically integrating eye-tracking with principles of foveal and peripheral vision, we address the severe visual occlusion limitations of traditional, full-field static guidance.
2. We implement a dynamic modulation mechanism (DSVG) that leverages real-time eye tracking to strictly confine stability cues to the foveal region. This engineering synthesis reduces visual occlusion by approximately 70% compared to the SVG baseline, successfully balancing sickness mitigation with a clear visual field.
3. We provide rigorous empirical validation through a comparative user study, demonstrating that DSVG significantly lowers subjective discomfort and improves physiological markers compared to a no-cue baseline, confirming the viability of fovea-restricted cues for adaptive RDW systems.

2 | Related Work

This section reviews the sensory conflicts in RDW and the physiological principles of vision that inform our proposed solution.

2.1 | Cybersickness in VR

Cybersickness remains a primary barrier to VR adoption, commonly explained by Sensory Conflict Theory [7]. Mismatches between vestibular signals and visual feedback—frequent during the gain manipulations of RDW—trigger symptoms including nausea and disorientation [8, 9]. To mitigate this, researchers have explored dynamic Field-of-View (FOV) restriction [10, 11], optical flow modulation [12], and peripheral motion cues [13]. However, these methods are often limited to static or vehicle-based scenarios [14, 15], with few solutions specifically optimized for the active locomotion of RDW. Assessment typically combines subjective measures, such as the Simulator Sickness Questionnaire (SSQ), with objective physiological signals like blink frequency and blood pressure [16, 17], which allow for continuous monitoring [18].

2.2 | Redirected Walking and Gains

RDW enables the exploration of large virtual environments within constrained physical spaces by manipulating user trajectories via gains [4]. While recent algorithms utilize potential fields [19, 20], predictive modeling [21, 22], and environmental analysis [23, 24] to optimize steering, they rely on rotation gains that correlate strongly with cybersickness [25]. Recent advancements have introduced standardized frameworks such as OpenRDW [26], which provides a comprehensive library and benchmark for state-of-the-art algorithms, including learning-based and multiuser functionalities in separate physical spaces [27]. While these frameworks focus on optimizing steering efficiency and hardware utilization, the intensified vestibular-visual mismatches caused by high gains—especially in constrained rooms—remain a critical barrier [28]. Our approach addresses this by providing a visual guidance layer that can be integrated into such systems to enhance user comfort without necessitating a reduction in gain magnitudes.

2.3 | Foveal Versus Peripheral Vision

Visual perception is hierarchically organized. The fovea (approx. 2°–5° eccentricity) provides high-acuity central vision crucial for detail [29], while the peripheral field specializes in motion detection and spatial orientation. Traditional visual cues often clutter the entire field of view, disrupting immersion. Leveraging the distinct roles of these regions, our DSVG renders stability cues exclusively in the fovea while fading them in the periphery. This bio-inspired approach aims to maintain redirection efficacy while minimizing visual occlusion.

3 | Method

This section details a method to mitigate cybersickness in RDW. We first introduce a basic steering visual cue prototype and then optimize it based on principles of central vision, peripheral vision, and the fovea to improve comfort and efficiency.

3.1 | Steering Visual Guidance Design

While static independent visual backgrounds have been utilized to reduce simulator sickness [6], they do not account for the continuous active locomotion in RDW. Therefore, we propose SVG

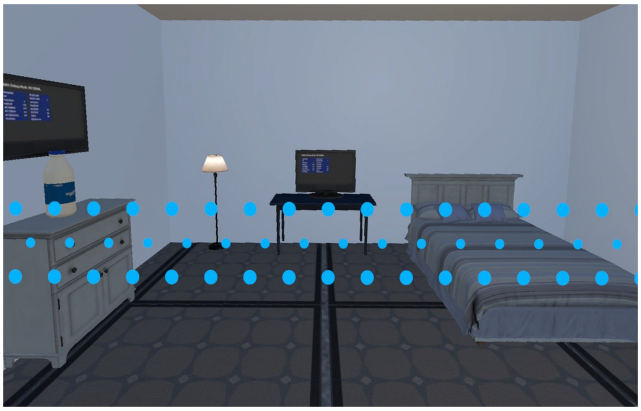

FIGURE 1 | Visuals of SVG.

as a dynamic evolution of this concept. The SVG interface comprises an array of light-blue circular cues, optimized for VR displays. Each cue subtends a visual angle of 0.8° and is arranged in three horizontally aligned rows. As shown in Figure 1, light blue—a low-luminance cool tone—was selected based on standard UI/UX guidelines for head-mounted displays (HMDs) because it minimizes visual strain and reduces eye fatigue during continuous VR exposure. The grid uses variable-density spacing to balance saliency and occlusion:The horizontal spacing between each cue is 8°, which makes the cues clearly distinguishable without forming a continuous texture, and vertical row positions follow a cosine falloff:

$$y_n = Y_{center} + (-1)^n \cdot 8.5^\circ \cdot \cos(\pi n/2), \tag{1}$$

where $n \in \{0, 1, 2\}$ denotes row index. 30% baseline transparency ensures foreground content visibility while maintaining guidance function. 8.5° indicates that the visual cue rows are positioned 8.5° above and below the central line of sight, respectively. The purpose is to distribute the visual cues within the user's central and near-peripheral visual field, a region that remains sensitive to overall motion direction and optic flow. This placement also avoids positioning the cues too close to the visual periphery, thereby establishing a spatially structured reference frame. The SVG plane is rigidly fixed to head-mounted display (HMD) coordinates at 2.0 m virtual depth, constrained to horizontal motion parallel to the naso-occipital axis. All angular units mentioned above are in degrees of visual angle.

When the user performs a redirected walk, the rotational gain will cause the virtual world to fail to reflect the user's real motion state, that is, it will not be consistent with the information perceived by the user's vestibule. This is the main cause of VR cybersickness. In order to correct the erroneous stimulation brought to the user by the visual information in the VR headset, the movement speed of the SVG needs to reflect the user's real physical motion state. That is, when the user rotates a certain angle, the SVG moves a certain distance in the corresponding direction, and both the direction and distance should follow the laws of the physical world.

We obtain the rotation state of each frame of the user during the VR experience, and by calculating the rotation difference between consecutive frames, we can obtain the angular velocity of the user's rotation at a certain moment. Then we can calculate the speed of the SVG based on the angular velocity and the distance of the SVG from the human eye.

The SVG's motion compensation adheres to body rotation-induced vestibulo-ocular dynamics. When the user rotates clockwise in physical space, visual projection displacement occurs in the counterclockwise direction relative to the HMD viewport. Conversely, counterclockwise body rotation triggers clockwise SVG displacement. This inverse mapping preserves retinal slip velocity within Vestibulo-Ocular Reflex (VOR) stabilization thresholds. The SVG is designed to move cyclically in front of the user's eyes, and is designed to move in a horizontal direction. is designed to move cyclically in front of the user's eyes, that is, no matter how many degrees the user rotates, the SVG will not go beyond the user's field of view.

$$\mathbf{V}_{SVG} = -\mathrm{sgn}(\langle \boldsymbol{\omega}_{phy}, \mathbf{e}_z \rangle) \cdot k_c \cdot \boldsymbol{\omega}_{phy} \times \mathbf{r}_{SVG}, \tag{2}$$

where $\mathbf{e}_z$ is the vertical axis unit vector, $k_c = 0.95$ is an empirical compensation factor. Instead of a formally benchmarked value, this heuristic parameter was determined through iterative pilot testing. We observed that applying a 5% dampening factor subjectively provided the most stable visual synchronization for the Pico 4 Pro headset, effectively compensating for minor, hardware-specific tracking discrepancies. Additionally, $\mathbf{r}_{SVG}$ is the distance of the SVG from the user's eyes in a VR virtual environment, as shown in Figure 2.

When the user rotates in the virtual world, the SVG automatically moves according to the specified speed. This movement is consistent with the real human motion, that is, with the user's vestibular perception. SVG indirectly guides the user's vision to the physical world, which greatly reduces the user's cybersickness symptoms.

3.2 | Optimization of SVG According to Vision Principles

To evaluate the foundational SVG model, we conducted a formative pilot study. Participants navigated a virtual environment using SVG with a rotation gain of 0.5. Based on subjective feedback and discomfort ratings (Figure 3), three key observations emerged:

First, SVG significantly attenuates cybersickness in RDW by providing a stable reference frame that aligns visual perception with vestibular cues. Second, however, a subset of users reported increased discomfort, attributing it to the high density and continuous motion of the grid pattern, which overwhelmed their visual processing. Finally, the full-field nature of the static SVG frequently occluded the virtual environment, obstructing the user's vision and preventing clear exploration of the scene.

To address the "comfort-vs.-occlusion" trade-off, we optimized the model by integrating physiological principles of human vision. Our objective was to minimize the negative visual impact of the guidance cues while preserving their stabilizing function.

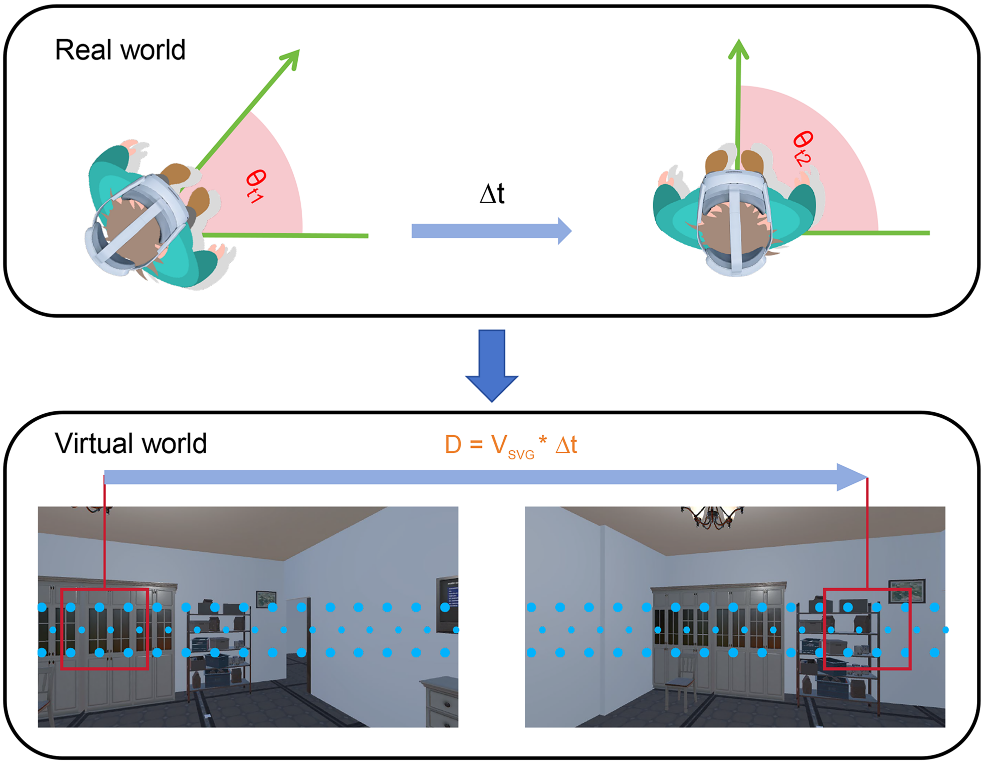

FIGURE 2 | How SVG works.

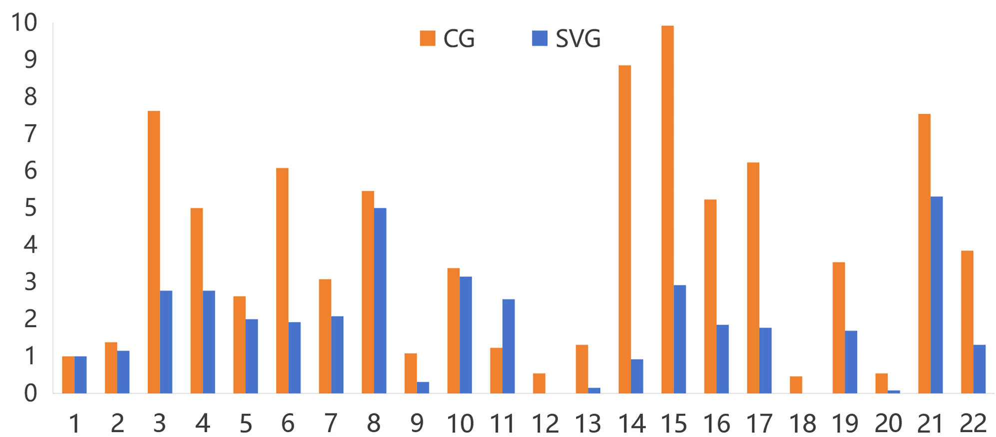

FIGURE 3 | Discomfort rating scale with SVG and no visual cues.

The first step was to solve the problem of increased cybersickness for some users. While visual acuity is highest in the fovea, the peripheral visual field is uniquely specialized for motion detection and processing global optic flow. Consequently, a dense, full-field array of moving patterns overwhelms these peripheral motion processing mechanisms, creating visual clutter that triggers visual fatigue and paradoxically increases discomfort for some users. By constraining the visual cues to the foveal region (DSVG), we provide a stable, VOR-compensated reference frame exactly where the user's conscious visual attention is anchored to mitigate sensory conflict. Simultaneously, we clear the periphery of artificial moving stimuli, allowing the visual system to naturally perceive the virtual environment's optic flow without obtrusive interference. In order to solve the above problems, we cropped the SVG to show only the moving blue dots in 30% of the user's field of view while the movement of the blue dots remains unchanged.

The blue dot is only displayed in the center of the field of view, and when the user's line of sight deviates from the center of the field of view, the user will not see the movement of the blue dot and will not receive the visual cue information. We utilize the eye-tracking feature so that the position of the blue dot always follows the position of the user's gaze point in the field of view. The visual cues are received no matter where the user looks in the field of view, as shown in Figure 4.

The blue dots have a 70% reduction in the display area, in order to maintain or improve its visual cue function and preserve the visibility of the virtual scene. We treat the blue dot based on

FIGURE 4 | Use eye tracking for visual cues.

the principle of the sensitivity relationship between central and peripheral vision. The center of the blue dot display area is taken as the origin, and its transparent gradient is over-processed. We give a formula for the relationship between the visual effect of the blue dot and the user's visual angle:

$$\alpha = \begin{cases} (i_{Cen} - k_{Cen}/(r+1))/d \\ \text{if } 0^\circ \leq r \leq 10^\circ \\ (i_{Per} - k_{Per} \cdot r)/d \\ \text{if } 10^\circ < r < 90^\circ \end{cases} \quad (3)$$

r denotes the visual angle, the angle from the observer's eye to a position in the image, α denotes the transparency of the blue dot, and d is the range of sensitivity in the sensitivity relationship between central and peripheral vision, which is used to normalize the calculation results of the molecule, so as to obtain the specific value of the transparency α.

Transparency (α) is modulated via a piecewise linear function based on visual eccentricity (r). In the central foveal region ($0^\circ \leq r \leq 10^\circ$), the cues remain predominantly opaque to provide a salient stabilizing anchor. Beyond this boundary ($10^\circ < r < 90^\circ$), transparency increases rapidly as a function of r, effectively fading the cues in the periphery where visual sensitivity is better tuned for natural optic flow.

However, because we cropped the display area of the blue dot, the effect of the blue dot in peripheral vision is not fully displayed. Central vision typically consists of a "fovea parafovea perifovea" with an outer boundary of approximately eccentricity, with a boundary dividing the central/peripheral region, consistent with the neurophysiological definition of visual partitioning [29]. We call the optimized visual cue model DSVG as shown in Figure 5.

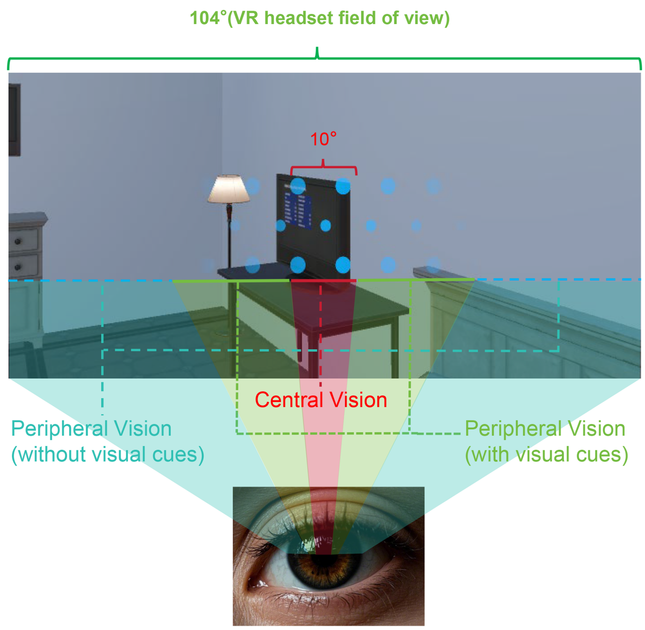

FIGURE 5 | Use visual principles to optimize the visual cue model.

4 | User Study

4.1 | Overview and Hypotheses

After completing the optimization of the static model, we obtained the final DSVG method. Our goal is to verify that the proposed DSVG method can reduce the occlusion of visual cues to the user's line of sight and reduce the user's cybersickness during RDW, and the effect demonstrates non-inferiority to SVG regarding sickness mitigation. To isolate the specific impact of our visual cues from other confounding factors, we evaluate SVG and DSVG against a standard baseline with no visual cues (Control Group, CG). This allows us to validate the progressive efficacy of our hierarchical design. Therefore, we propose the following hypothesis:

Hypothesis 1. *Visual guidance (both SVG and DSVG) significantly mitigates cybersickness compared to navigating without visual cues.*

Hypothesis 2. *Visual guidance (both SVG and DSVG) significantly increases the comfortable walking duration compared to navigating without visual cues.*

Hypothesis 3. *Fovea-restricted guidance (DSVG) is non-inferior to full-field guidance (SVG) regarding sickness mitigation and comfort duration.*

4.2 | Participants and Apparatus

We recruited 22 participants, 13 males and 9 females, aged between 23 and 29 years (Mean = 23.875, SD = 1.46). Vision was

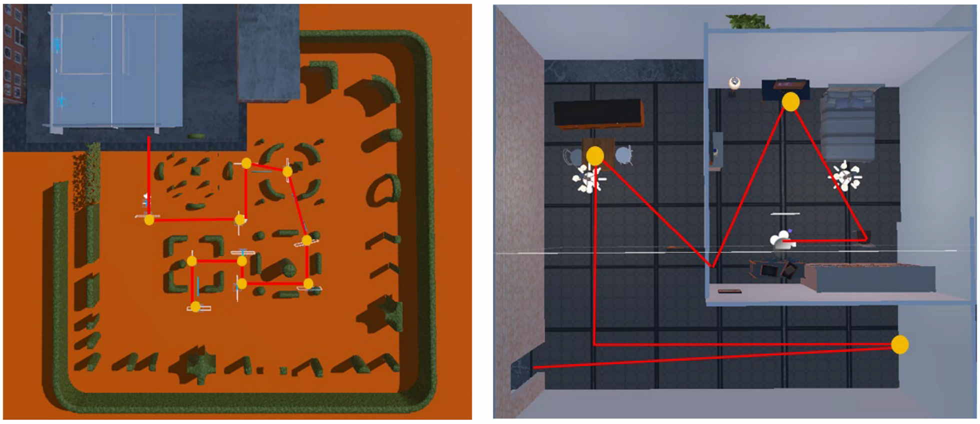

FIGURE 6 | Virtual outdoor environment on left and indoor environment on right.

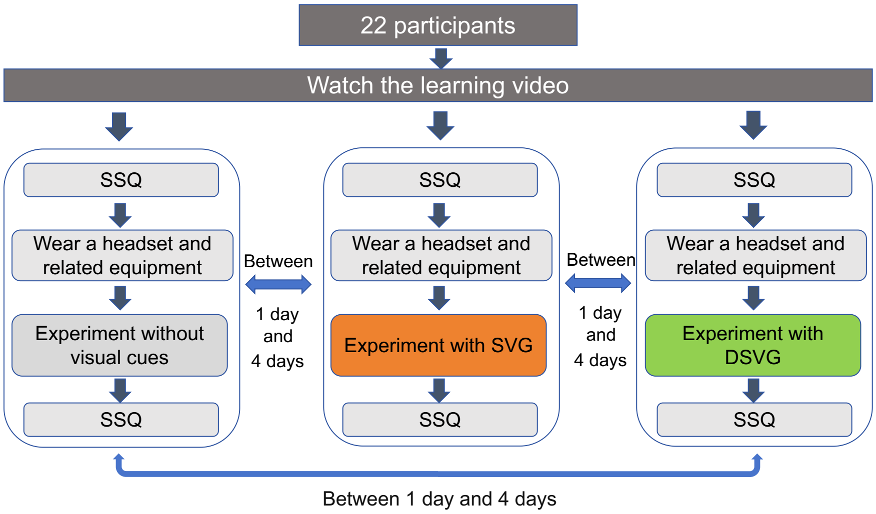

FIGURE 7 | Participants' experimental program.

normal. Sixteen of them had experience with HMD VR applications and none reported balance disorders. A post hoc power analysis indicated that with $N = 22$, an alpha level of 0.05, and the observed large effect sizes (all partial eta squared $\eta_p^2 > 0.40$), the statistical power $(1 - \beta)$ to detect the main effects of the visual conditions exceeded 0.90, confirming that the study was adequately powered. The HMD device used in our system was the Pico 4 Pro, which has 6 DoF spatial localization, automatic pupil adjustment, eye tracking, and face tracking. The above features can detect the user's eye position and blink information. We packaged the experimental program to run on the HMD without using a computer. We used the 24-hour ambulatory blood pressure monitor to collect the user's blood pressure and pulse information. The measurable blood pressure range is 0-299 mmHG with a margin of error of 3 $\pm$ mmHG. The measurable pulse rate is 40-190/min with a margin of error of $\pm$ 3% of the readout. The frequency of measurement is 2 mins. None of the $N = 22$ participants in the main study had taken part in the initial SVG pilot test.

4.3 | Experimental Environment

The experimental platform was developed in Unity, simulating a seamless indoor–outdoor environment navigated from a first-person perspective. To evaluate the efficacy of visual guidance under stress, we applied a constant, strictly rotational gain of 0.5 (with no translational or curvature gains applied). The trajectory consists of 13 sequential waypoints (3 indoor, 10 outdoor; see Figure 6). Indoor tasks included object manipulation and a mental arithmetic challenge requiring continuous 180° rotation, specifically designed to induce vestibular-visual conflict. Outdoor traversal focused on long-distance locomotion. Upon reaching each waypoint, a UI prompt requested a real-time discomfort rating (0–10 scale) via a controller-driven slider. The study was conducted in a 2700m^2 obstacle-free physical space to ensure unhindered large-scale redirection.

4.4 | User Study Design

Figure 7 shows the experimental protocol. Each participant was required to perform three experiments, and the three experiments corresponded to three different experimental configurations (no visual cues, using SVG, and using DSVG). The order between the three experiments was randomized. The virtual and physical environments and the tasks completed were the same for each experiment. The interval between the two experiments performed by the same participant was at least greater than 1 day, but not more than 4 days. This was done to minimize interactions between the two experiments.

Each participant was required to complete a pre-exposure SSQ before conducting the experiment, followed by viewing an instructional video that explained how to use the joystick to complete tasks in the VR virtual environment and the perceived differences between the VR virtual world and the physical world. Users wore a Cloudsea 24-hour ambulatory blood pressure monitor to collect information about their blood pressure and pulse rate. At the beginning of the experiment, participants wore a headset device to move around using an RDW system and complete the tasks we set. For each task, users were asked to answer a discomfort score that appeared in front of them. Participants were informed in advance that if they reached a discomfort score of 10 or reported that the cybersickness was too strong to continue the experiment, their participation would be immediately terminated. Remaining unanswered discomfort scores were assigned a default value of 10. The experiment was terminated when the participant reached the last path point. Upon completion or termination of the experiment, participants were asked to complete the Post-Exposure SSQ.

4.5 | Experimental Indicators and Results

All participants' cybersickness was quantified using the following subjective and objective metrics: before and after SSQ score difference, discomfort score, number of path points completed, blinking frequency, blood pressure, and pulse rate. The difference between the pre- and post-SSQ scores served as a secondary metric because the SSQ was collected before and after the participants performed the experiment, and it did not take into account what the participants felt in real time in the VR virtual environment, which may not accurately reflect the participants' sense of cybersickness. The discomfort score was used as a primary subjective indicator. The number of path points completed indicated the quality of the task completed by the participant. Blink frequency, blood pressure, and pulse rate are physiological indicators for evaluating cybersickness, and these indicators need to be measured in real time while the participant is performing the experiment.

To rigorously evaluate the condition effects within our repeated-measures design, we adopted a comprehensive hierarchical statistical framework. First, a one-way Repeated-Measures ANOVA (RM-ANOVA) was conducted for all continuous metrics to determine the significance of the overall main effects, with results reported via F-values and partial eta squared (η_p^2) for effect size estimation. Following the identification of significant main effects, we performed detailed pairwise comparisons using t-tests across the three experimental conditions (CG vs. SVG, CG vs. DSVG, and SVG vs. DSVG). To manage the inflated Type I error rate associated with multiple comparisons, a Bonferroni correction was applied, resulting in an adjusted significance threshold of $\alpha = 0.05/3 = 0.017$. Furthermore, to specifically test the non-inferiority claims in H3, we supplemented these frequentist analyses with Bayesian statistical tests to evaluate the strength of evidence between the SVG and DSVG conditions.

4.5.1 | Discomfort Score

User experiments examined the differences in discomfort scores between the use of SVG and DSVG and the absence of visual aids. Figure 8 shows a graphical representation of the score difference.

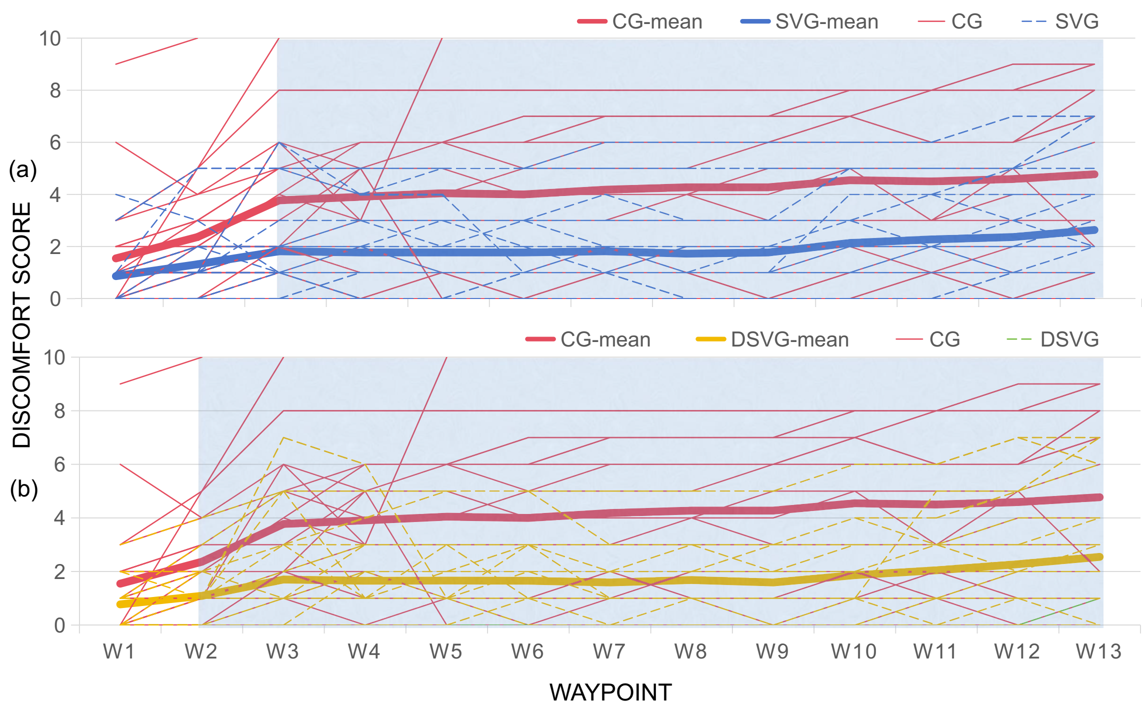

FIGURE 8 | Discomfort scores for each participant as a function of pathway point and the mean discomfort score for each pathway point in each experimental condition. (a) CG versus SVG, (b) CG versus DSVG. areas indicate path points with statistically significant differences.

Table 1 shows the statistical results. In Figure 8a, the vertical axis corresponds to the discomfort score, with lower scores representing greater comfort. The horizontal axis represents path points, and the use of path points ensures that participants experience the same virtual environment stimuli when reporting the discomfort scores. The thin red line indicates participants to whom visual cues did not apply, and the thin blue line indicates participants who used SVG. Participants to whom visual cues did not apply were averaged over the path points, indicated using the thick red line, and participants using SVG were averaged over the path points, indicated using the thick blue line. In Figure 8b, the same method was used to compare participants with no visual cues applied and participants with DSVG.

Pairwise comparisons indicated that the SVG-mean ($M = 1.85$) was significantly lower than the CG-mean ($M = 3.91$). The discomfort scores of participants using SVG were significantly lower than those navigating without visual cues, successfully supporting our Hypothesis H1. Similarly, the DSVG-mean ($M = 1.79$) was also significantly lower than the CG baseline, providing further corroboration for H1. These robust pairwise differences were comprehensively validated by an RM-ANOVA, which revealed a highly significant overall main effect of the visual guidance condition on discomfort scores, $F(2, 42) = 18.09, p < 0.001, \eta_p^2 = 0.46$. Furthermore, we compared the specific performance gap between SVG and DSVG, as detailed in Table 2. According to the Bayesian factor, even when the dynamic visual cue reduces the display area by 70%, the mitigating effect of DSVG is not significantly different from – and may even slightly exceed – that of the full-field SVG. This confirms the non-inferiority of our dynamic approach, fully supporting our Hypothesis H3.

TABLE 1 | Discomfort score results for each method. * denote statistica significance.

Method	Avg. ±std. dev.	$\frac{\|M_i - M_{CG}\|}{M_{CG}}$	p	t	Cohen's d	Effect size
CG	3.91 ± 2.84					
SVG	1.85 ± 1.42	53.5%	< 0.017*	2.969	0.92	Large
DSVG	1.79 ± 1.42	54.2%	< 0.017*	3.053	0.94	Large

TABLE 2 | Comparison of discomfort scores between SVG and DSVG. * denote statistica significance.

Method	Avg. ±std. dev.	$\frac{\|M_i - M_{CG}\|}{M_{CG}}$	Bayes factor
SVG	1.85 ± 1.42		
DSVG	1.79 ± 1.42	3.3%	0.311

4.5.2 | Number of Waypoints Completed

Due to the fact that the movement patterns of the participants during the experiment were rather complex, we regarded the total number of waypoints completed in each experiment as a representation of the comfortable duration during the experiment. We measured the number of waypoints completed by each user and analyzed them, and Figure 9 gives a graphical result.

The number of waypoints completed by the participants when using SVG was significantly higher than that completed by the participants who did not use visual cues. Three participants could not complete all the path points without visual cues, but successfully completed the entire experiment with the help of SVG. This verified our Hypothesis H2. There was no decrease in the performance of participants using DSVG compared to those using SVG, and all participants using DSVG completed all the waypoints we set. This validates hypotheses H2 and H3. However, it cannot be concluded that the effect of DSVG is greater than that of SVG, which reflects some shortcomings in our experimental design.

4.5.3 | Blink Frequency

We used the built-in expression detection feature of HMD to collect participants' blink data. The results of the experiment are shown in Figure 10 and the statistical results are also given in Table 3.

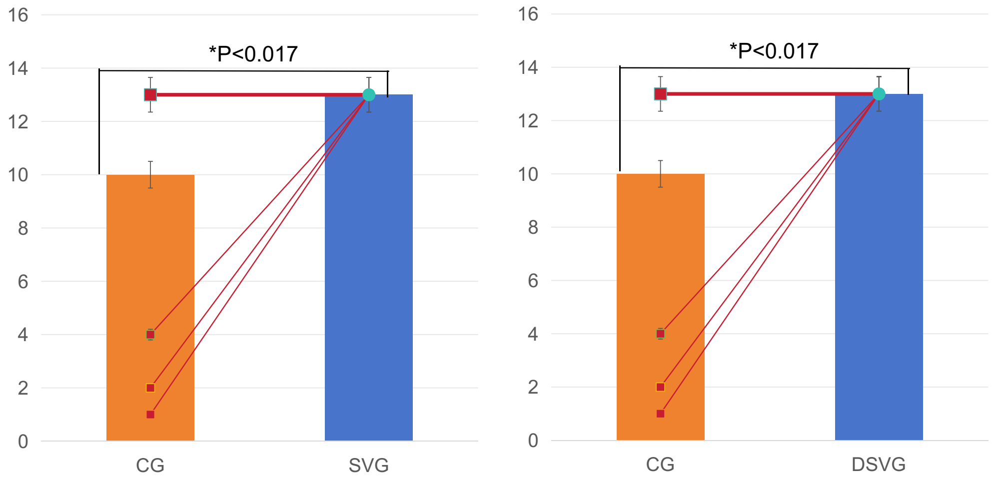

FIGURE 9 | Mean and individual completed waypoints. Bars represent averages, while red lines track individual participant trajectories across conditions.

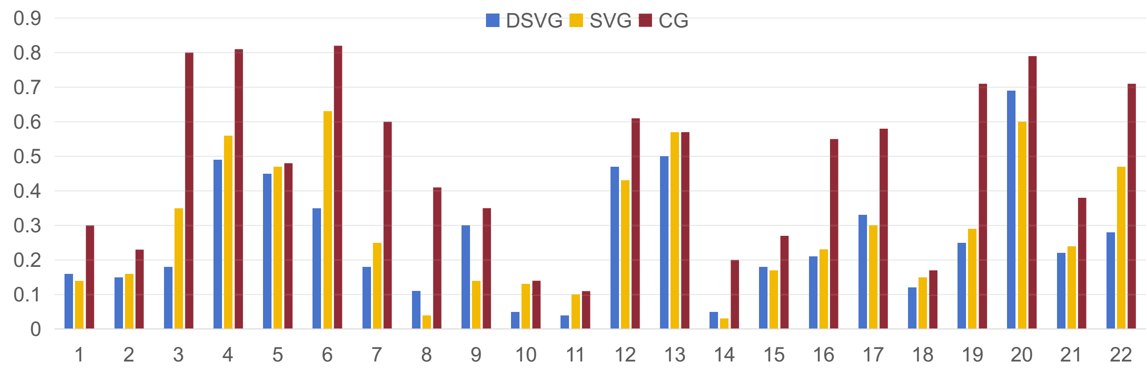

FIGURE 10 | Blink frequency for each participant in different experimental conditions.

TABLE 3 | Statistical results for different indicators (compared to CG).

Standards	Method	Avg. ±std. dev.	$\frac{\lvert M_i - M_{CG} \rvert}{M_{CG}}$	p	t	Cohen's d	Effect size
	CG	0.48±0.23					
Blink Frequency	SVG	0.29±0.18	39.6%	< 0.017*	2.914	0.90	Large
	DSVG	0.26±0.16	45.8%	< 0.001**	3.522	1.07	Large
	CG	9.09±8.46					
SSQ score	SVG	3.81±3.91	58.1%	< 0.017*	2.591	0.80	Large
	DSVG	3.18±3.74	65.0%	< 0.017*	2.925	0.90	Large
	CG	28.03±0.68					
SD of PSD_{SYS}	SVG	28.87±1.26	2.9%	< 0.0173	2.535	0.85	Large
	DSVG	28.89±0.73	3.1%	< 0.001**	3.728	1.24	Very Large
	CG	28.47±1.08					
SD of PSD_{PR}	SVG	28.99±0.84	1.8%	0.12	1.611	0.54	Medium
	DSVG	28.71±1.15	0.8%	0.52	0.650	0.22	Small

An RM-ANOVA demonstrated a highly significant overall main effect of the experimental conditions on blink frequency, $F(2, 42) = 32.18, p < 0.001, \eta_p^2 = 0.61$. Subsequent pairwise comparisons revealed that, compared with participants who navigated without visual cues, the blinking frequencies of those using SVG and DSVG significantly decreased during the experiment. Specifically, we observed a 39.6% decrease in blink frequency in the SVG group and a 45.8% decrease in the DSVG group, successfully confirming our Hypothesis H1. Furthermore, Table 4 details the specific comparison between the two guidance methods, highlighting an additional 10% reduction in blink frequency for the DSVG group compared to the SVG group. Supported by the Bayesian factor analysis, this finding not only confirms our Hypothesis H3 regarding non-inferiority, but also reflects an enhanced mitigating effect of DSVG on visual fatigue compared to the static SVG.

4.5.4 | SSQ

We collected SSQ reports from each user before and after the trial. The experimental results are shown in Figure 11, and the statistical results are also presented in Table 3.

TABLE 4 | Statistical results of different indicators (DSVG vs. SVG).

Standards	$\frac{\lvert M_{SVG} - M_{DSVG} \rvert}{M_{DSVG}}$	Bayes factor
Blink frequency	10.3%	0.114
SSQ score	16.5%	0.178
SD of PSD_{SYS}	3.1%	0.125
SD of PSD_{PR}	0.96%	0.416

The subjective improvements in cybersickness were strongly validated by the supplementary RM-ANOVA, which indicated a significant main effect of the visual conditions on SSQ score increments, $F(2, 42) = 15.40, p < 0.001, \eta_p^2 = 0.42$. Pairwise comparisons revealed that participants using either SVG or DSVG exhibited significantly lower SSQ increments compared to those navigating without visual aids, yielding large effect sizes (Cohen's d) and thereby supporting our Hypothesis H3. Furthermore, comparing DSVG directly with SVG (as detailed in Table 4) revealed no statistically significant difference between the two guided groups. The substantial effect size of DSVG relative to the control, combined with its comparable performance to the full-field SVG, confirms the non-inferiority of our fovea-restricted

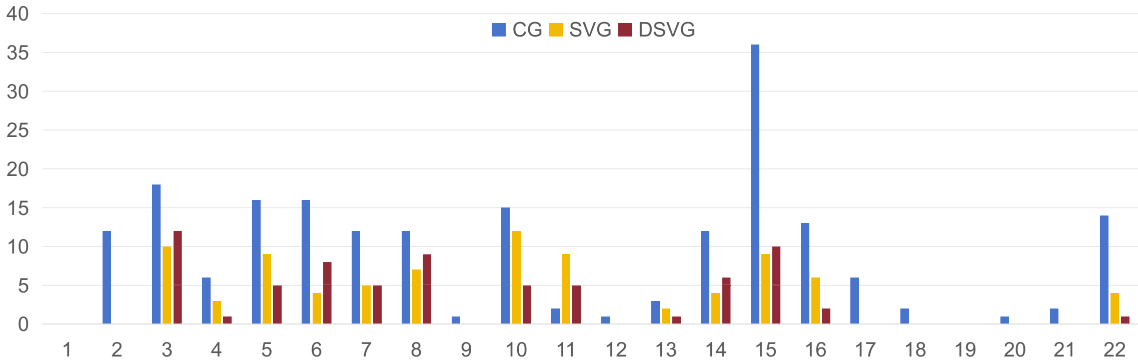

FIGURE 11 | SSQ Score for each participant in different experimental conditions.

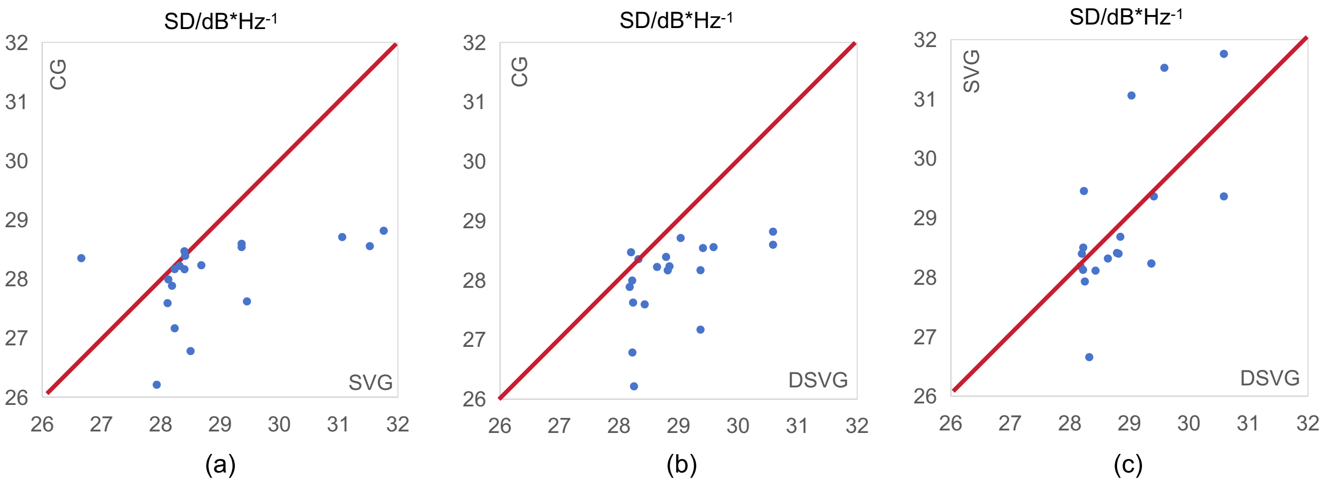

FIGURE 12 | PSD_{SYS} for each participant in different experimental conditions.

approach. This perfectly aligns with our Bayesian factor analysis and fully supports our Hypothesis H3.

4.5.5 | Blood Pressure

According to [18], the standard deviation of power frequency density of systolic blood pressure (PSD_{SYS}) (in dB/Hz) is a physiological indicator that can reflect cybersickness in the frequency domain, and the standard deviation of PSD_{SYS} is negatively correlated with cybersickness of the participants, which means that the smaller the standard deviation of PSD_{SYS} is, the more the participants' cybersickness is. The collected systolic blood pressure data were processed, and the results are shown in Figure 12 and the statistical results are presented in Tables 3 and 4.

The standard deviation of PSD_{SYS} increased significantly under the effect of SVG. As shown in Figure 12a, most of the points are located on the underside of the diagonal. The standard deviation of PSD_{SYS} increases significantly under the action of DSVG, as shown in Figure 12b, where most of the points are distributed on the lower side of the diagonal. Combined with the statistical results in Tables 3 and 4, our hypotheses H1 is validated. The standard deviation of PSD_{SYS} is not much different under the influence of SVG and DSVG. As shown in Figure 12c, the majority of points are distributed around the diagonal, which validates our Hypothesis H3.

4.5.6 | Pulse Rate

Pulse rate is similar to blood pressure, and we need to calculate the standard deviation of the power frequency density (PSD_{PR}) of the pulse rate. The standard deviation of the PSD_{PR} is negatively correlated with the cybersickness of the participants. Figure 13 shows the experimental results, and Tables 3 and 4 also give the statistical results. We performed the T-test on the data between the different groups, and the p-values were 0.12 and 0.52, respectively, with no statistically significant differences. In Figure 13a–c, we can see that the distribution of points does not show much regularity. This lack of statistical significance is primarily attributed to the physical walking interference inherent to our RDW tasks. The continuous active locomotion introduced significant physical exertion noise and motion artifacts into the pulse rate measurements. Consequently, without the application of advanced signal filtering techniques, the raw pulse rate data is overwhelmingly dominated by the participants' motor status, making it difficult to accurately isolate and reflect the specific physiological symptoms of cybersickness.

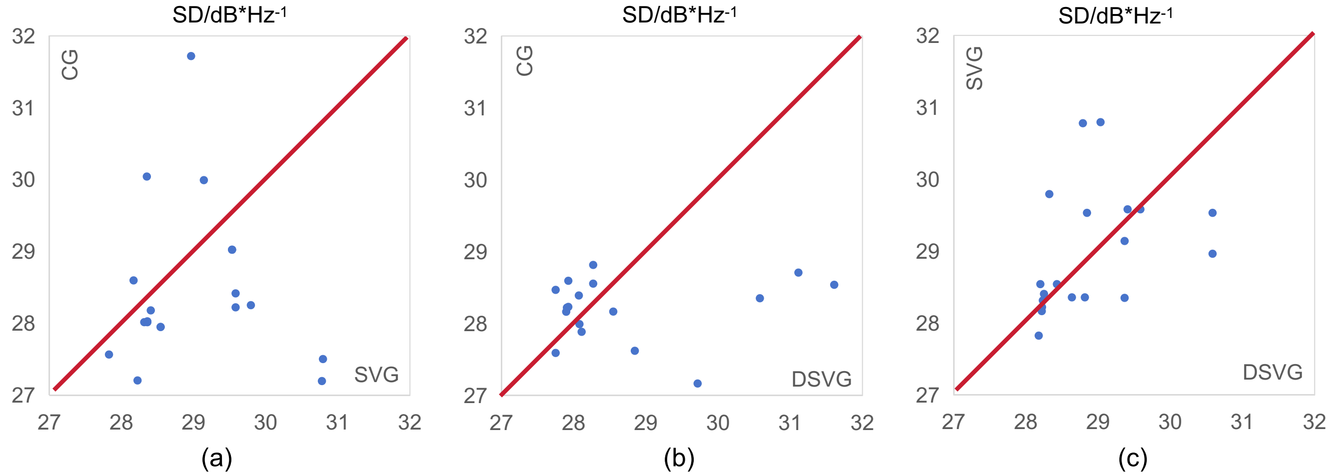

FIGURE 13 | PSD_{PR} for each participant in different experimental conditions.

5 | Conclusion and Limitation

This study introduces Dynamic Steering Visual Guidance (DSVG), a novel gaze-contingent framework designed to mitigate cybersickness in RDW. By aligning visual cues with the physiological sensitivity of foveal and peripheral vision, DSVG resolves the trade-off between comfort and visual occlusion. Our empirical results demonstrate that DSVG is non-inferior to static guidance (SVG) in reducing subjective discomfort and physiological stress markers, while significantly minimizing visual occlusion. This confirms that bio-inspired visual suppression is a viable pathway for enhancing the practicality of RDW in constrained physical spaces.

However, this study has notable limitations regarding the evaluation of user experience. Our experimental design primarily focused on quantifying cybersickness mitigation through objective physiological markers and basic subjective metrics. We did not conduct formal qualitative interviews, nor did we employ standardized psychometric questionnaires (e.g., the Igroup Presence Questionnaire) to directly measure user immersion, presence, or qualitative preferences. Consequently, while DSVG significantly reduces geometric visual occlusion, its specific psychological impact on the sense of presence remains to be fully quantified. Future work will incorporate comprehensive qualitative assessments and subjective usability evaluations to provide a more holistic understanding of dynamic visual guidance.

Additionally, certain system parameters, such as the hardware compensation factor, were determined empirically through pilot testing; future deployments would benefit from rigorous, standardized hardware benchmarking to optimize these values. Furthermore, our findings regarding pulse rate highlight a critical methodological limitation: measuring cardiovascular metrics during active VR locomotion is highly susceptible to physical interference. Future RDW studies must incorporate advanced signal filtering algorithms to successfully decouple cybersickness-induced physiological responses from typical motion artifacts.

Author Contributions

Xinda Liu: writing – original draft, conceptualization. **Yongbo Tang:** writing – original draft, conceptualization. **Xiaoning Liu:** writing – review and editing, methodology. **Pengbo Zhou:** writing – review and editing. **Guohua Geng:** visualization, funding acquisition.

Acknowledgments

This work was supported by the National Key Research and Development Program of China (Grant No. 2024YFF0907605), the General Projects of the Shaanxi Provincial Department of Science and Technology (Grant No. 2025JC-YBQN-801), and the Shaanxi Provincial Natural Science Basic Research Program (Grant No. 2025JC-YBMS-706). The authors sincerely acknowledge the funding support from all the above programs, which provided a solid guarantee for the smooth implementation of this research.

Funding

This work was supported by the National Key Research and Development Program of China (Grant No. 2024YFF0907605), the General Projects of the Shaanxi Provincial Department of Science and Technology (Grant No. 2025JC-YBQN-801), and the Shaanxi Provincial Natural Science Basic Research Program (Grant No. 2025JC-YBMS-706).

Ethics Statement

The experimental protocol was reviewed and approved by the Ethics Committee of Northwest University (Approval No. 241113089). Prior to the study, all participants were thoroughly informed about the experimental procedures, including the specific risks of experiencing cybersickness during the RDW tasks. Written informed consent was obtained from all participants. Furthermore, participants were explicitly instructed that they had the right to terminate the experiment at any time without penalty if they experienced severe discomfort.

During the preparation of this work, the authors used artificial intelligence tools solely to improve the English language and readability of the manuscript. After using these tools, the authors reviewed and edited the content as needed and take full responsibility for the content of the publication.

Conflicts of Interest

The authors declare no conflicts of interest.

Data Availability Statement

The data that support the findings of this study are available on request from the corresponding author. The data are not publicly available due to privacy or ethical restrictions.

References

1. F. Steinicke, G. Bruder, J. Jerald, H. Frenz, and M. Lappe, "Estimation of Detection Thresholds for Redirected Walking Techniques," *IEEE Transactions on Visualization and Computer Graphics* 16, no. 1 (2009): 17–27.

2. E. A. Suma, Z. Lipps, S. Finkelstein, D. M. Krum, and M. Bolas, "Impossible Spaces: Maximizing Natural Walking in Virtual Environments With Self-Overlapping Architecture," *IEEE Transactions on Visualization and Computer Graphics* 18, no. 4 (2012): 555–564.

3. C. T. Neth, J. L. Souman, D. Engel, U. Kloos, H. H. Bulthoff, and B. J. Mohler, "Velocity-Dependent Dynamic Curvature Gain for Redirected Walking," *IEEE Transactions on Visualization and Computer Graphics* 18, no. 7 (2012): 1041–1052.

4. Y.-J. Li, F. Steinicke, and M. Wang, "A Comprehensive Review of Redirected Walking Techniques: Taxonomy, Methods, and Future Directions," *Journal of Computer Science and Technology* 37, no. 3 (2022): 561–583.

5. B. Williams, G. Narasimham, B. Rump, et al., "Exploring Large Virtual Environments With an HMD When Physical Space Is Limited," in *Proceedings of the Symposium on Applied Perception in Graphics and Visualization* (ACM, 2007), 41–48.

6. H. B.-L. Duh, D. E. Parker, and T. A. Furness, "An Independent Visual Background Reduced Balance Disturbance Evoked by Visual Scene Motion: Implication for Alleviating Simulator Sickness," in *Proceedings of the SIGCHI Conference on Human Factors in Computing Systems, CHI'01* (ACM, 2001), 85–89.

7. J. T. Reason and J. J. Brand, *Motion Sickness*, vol. 1 (Academic Press, 1975).

8. J. F. Golding, "Predicting Individual Differences in Motion Sickness Susceptibility by Questionnaire," *Personality and Individual Differences* 41, no. 3 (2006): 237–248.

9. C. M. Oman, "Motion Sickness: A Synthesis and Evaluation of the Sensory Conflict Theory," *Canadian Journal of Physiology and Pharmacology* 68, no. 2 (1990): 294–303.

10. I. B. Adhanom, N. N. Griffin, P. MacNeilage, and E. Folmer, "The Effect of a Foveated Field-Of-View Restrictor on VR Sickness," in *IEEE Conference on Virtual Reality and 3D User Interfaces (VR)* (IEEE, 2020), 645–652.

11. C. H. Lim and S. C. Lee, "The Effects of Degrees of Freedom and Field of View on Motion Sickness in a Virtual Reality Context," *International Journal of Human Computer Interaction* 40, no. 19 (2024): 5884–5896.

12. P. Bala, I. Oakley, V. Nisi, and N. Nunes, "Staying on Track: A Comparative Study on the Use of Optical Flow in 360 Video to Mitigate Vims," in *Proceedings of the ACM International Conference on Interactive Media Experiences* (ACM, 2020), 82–93.

13. E. Kim, H. Gil, J. Ryu, I. Oakley, and G. Shin, "The Effect of Peripheral Cues on Motion Sickness Mitigationwhen Using a VR HMD in a Car," in *Proceedings of the Human Factors and Ergonomics Society Annual Meeting*, vol. 66 (SAGE Publications Sage CA, 2022), 1967–1971.

14. R. Lou, F. Mérienne, and D. Bechmann, "General Framework of Geometric Simplification for Mitigating Cybersickness," in *International Conference on Future Trends in Smart Communities (ICFTSC)* (IEEE, 2022), 1–5.

15. A. K. T. Ng, L. K. Y. Chan, and H. Y. K. Lau, "A Study of Cybersickness and Sensory Conflict Theory Using a Motion-Coupled Virtual Reality System," *Displays* 61 (2020): 101922.

16. R. Liu, E. Peli, and A. D. Hwang, "Measuring Visually Induced Motion Sickness Using Wearable Devices," *Electronic Imaging* 29 (2017): 218–223.

17. P. Lopes, N. Tian, and R. Boulic, "Exploring Blink-Rate Behaviors for Cybersickness Detection in vr," in *IEEE Conference on Virtual Reality and 3D User Interfaces Abstracts and Workshops (VRW)* (IEEE, 2020), 794–795.

18. Y. Lin, R. Jia, R. Liu, and T. Chen, "Assessment Metrics for Visually Induced Motion Sickness in Virtual Reality Environments," *Aerospace Medicine and Medical Engineering* 31, no. 4 (2018): 9.

19. E. R. Bachmann, E. Hodgson, C. Hoffbauer, and J. Messinger, "Multi-User Redirected Walking and Resetting Using Artificial Potential Fields," *IEEE Transactions on Visualization and Computer Graphics* 25, no. 5 (2019): 2022–2031.

20. J.-J. Chen, H.-C. Hung, Y.-R. Sun, and J.-H. Chuang, "APF-S2T: Steering to Target Redirection Walking Based on Artificial Potential Fields," *IEEE Transactions on Visualization and Computer Graphics* 30 (2024): 2464–2473.

21. B. J. Congdon and A. Steed, "Monte-Carlo Redirected Walking: Gain Selection Through Simulated Walks," *IEEE Transactions on Visualization and Computer Graphics* 29, no. 5 (2023): 2637–2646.

22. S.-B. Jeon, J. Jung, J. Park, and I.-K. Lee, "F-RDW: Redirected Walking With Forecasting Future Position," *IEEE Transactions on Visualization and Computer Graphics* 31 (2024): 1970–1984.

23. N. L. Williams, A. Bera, and D. Manocha, "Arc: Alignment-Based Redirection Controller for Redirected Walking in Complex Environments," *IEEE Transactions on Visualization and Computer Graphics* 27, no. 5 (2021): 2535–2544.

24. N. L. Williams, A. Bera, and D. Manocha, "Eni: Quantifying Environment Compatibility for Natural Walking in Virtual Reality," in *IEEE Conference on Virtual Reality and 3D User Interfaces (VR)* (IEEE, 2022), 419–427.

25. N. L. Williams and T. C. Peck, "Estimation of Rotation Gain Thresholds Considering Fov, Gender, and Distractors," *IEEE Transactions on Visualization and Computer Graphics* 25, no. 11 (2019): 3158–3168.

26. Y.-J. Li, M. Wang, F. Steinicke, and Q. Zhao, "Openrdw: A Redirected Walking Library and Benchmark With Multi-User, Learning-Based Functionalities and State-of-the-Art Algorithms," in *Proceedings of the 2021 IEEE International Symposium on Mixed and Augmented Reality (ISMAR)* (IEEE, 2021), 21–30.

27. T. Dong, T. Gao, Y. Dong, L. Wang, H. Kefan, and J. Fan, "Free-Rdw: A Multi-User Redirected Walking Method for Supporting Non-Forward Steps," *IEEE Transactions on Visualization and Computer Graphics* 29, no. 5 (2023): 2315–2325.

28. C. A. Tirado Cortes, H.-T. Chen, and C.-T. Lin, "Analysis of vr Sickness and Gait Parameters During Non-Isometric Virtual Walking With Large Translational Gain," in *Proceedings of the 17th ACM SIGGRAPH International Conference on Virtual-Reality Continuum and its Applications in Industry* (ACM, 2019), 1–10.

29. L. C. Loschky, S. Szaffarczyk, C. Beugnet, M. E. Young, and M. Boucart, "The Contributions of Central and Peripheral Vision to Scene-Gist Recognition With a 180 Visual Field," *Journal of Vision* 19, no. 5 (2019): 15.